A&A 442, 673–685 (2005)
DOI: 10.1051/0004-6361:20042620

Astronomy & Astrophysics

Proton and helium release times in SEP events observed with SOHO/ERNE

K. Huttunen-Heikinmaa, E. Valtonen, and T. Laitinen

Space Research Laboratory, Department of Physics, University of Turku, 20014 Turku, Finland
e-mail: kahehu@utu.fi

Received 28 December 2004 / Accepted 19 May 2005

ABSTRACT

We determine the proton and helium nuclei release times at the Sun for 25 SEP events within the time period May 8, 1996–June 20, 2001, and compare them to each other. The event onset times at 1 AU are determined with a Poisson-CUSUM method, and the solar release times are obtained by the velocity dispersion analysis. Velocity dispersions were derived in the energy range 14–51 MeV/n. If the release times of protons and helium nuclei do not overlap within their error limits, and if protons are released earlier than helium, then the helium event is defined as "delayed". Seventeen helium events (68%) were found to be "delayed" and only eight (32%) "non-delayed". The average delay was (34 ± 18) minutes. The event-related flare location had an important role in the "non-delayed" events. A significant difference was found in the helium-to-proton ratios at the time of maximum intensity of the "delayed" and "non-delayed" events. No clear evidence was found that the "delayed" and "non-delayed" events would correspond the classical gradual-impulsive division of SEP events. We find that the delay is related to the poor magnetic connection between the flare site and the spacecraft.

Key words. acceleration of particles – methods: data analysis – Sun: coronal mass ejections (CMEs)

1. Introduction

Knowledge of the injection time of solar energetic particles (SEP) at the Sun is crucial when deducing the acceleration processes in action. Inferring the release time from in situ observations at 1 AU has turned out to be difficult, due to the many unknown variables: what is the actual length and shape of the magnetic field line along which the particles propagate? What are the conditions of interplanetary transport of the particles? What is the actual injection profile – a longer-lasting injection leads to a later onset in interplanetary space (Kallenrode & Wibberenz 1990). How are the neutral lines ordered and what is the angular distance between the flare and the observer's magnetic footpoint – neutral lines strongly influence the time scales of the azimuthal spread of particles and the observed particle event onset is more delayed with increasing angular distance (Kallenrode 1993; similar delays were also found from out of ecliptic observations by Dalla et al. 2003). On the other hand, the observation of the exact event onset time poses clear difficulties. Low sensitivity of the instrument or low signal-to-noise ratio (high background) at the very beginning of the event may lead to a delay in the observed onset. Also the instrument response can cause uncertainties in the results (Haggerty & Roelof 2003). Furthermore, all the uncertainties may be dependent on the particle energy and species.

Despite of the difficulties, several investigations with varying goals relying on SEP event onset analysis have been carried out fairly recently (Kahler 1994; Debrunner et al. 1997; Torsti et al. 1998; Krucker et al. 1999; Laitinen et al. 2000; Krucker & Lin 2000; Hilchenbach et al. 2003; Haggerty & Roelof 2002; Tylka et al. 2003; Posner & Kunow 2003; Mewaldt et al. 2003; Ho et al. 2003; Dalla et al. 2003). Specifically, temporal relations of SEP event onsets with solar radio or other electromagnetic emissions and differences in the onsets of various SEP species have been studied. Krucker et al. (1999) studied the solar release times of electrons in impulsive events and compared them to the onsets of radio type III bursts by using observations from the Wind spacecraft. In some events the injection time of the electrons was found to be consistent with the timing of the type III radio emission, while in other cases the electrons were released up to half an hour later than the onset of the type III burst. Haggerty & Roelof (2002) presented analysis of the timing between the near-relativistic electron injection and the soft X-ray, microwave, chromospheric Hα, and type III radio emission. They concluded that the near-relativistic electrons associated with western hemisphere events measured by the ACE spacecraft were injected with a median delay of ~10 min after the start of the electromagnetic emissions.

By using Wind observations, Krucker & Lin (2000) investigated the timing of proton onsets in the energy range from ~30 keV to 6 MeV and compared them to the release of 1–300 keV electrons. As a result, two classes of solar proton events were discovered. One type of events had apparent

path lengths 1.1−1.3 AU for both species, but protons were injected ∼0.5−2 h later than electrons. The second type of events showed nearly simultaneous injection of protons and electrons, but longer path lengths of about 2 AU for protons, and "nominal" path lengths (1.1−1.3 AU) for electrons. More recently, Mewaldt et al. (2003) compared the release times of heavy ions ($Z \geq 6$; 6−88 MeV/n) and electrons (38−315 keV) using ACE data. They found that heavy ions were generally released later than electrons, by as much as ∼50 min, and that there was an apparent correlation between the release times and the ^{3}He/^{4}He ratio. Events with ^{3}He/^{4}He > 0.02 had similar ion and electron release times and appeared to be released within 2 $R_\odot$ of the solar surface, while those with ^{3}He/^{4}He < 0.02 had greater ion-electron timing differences and appeared to be released ∼2 $R_\odot$ to ∼10 $R_\odot$ from the Sun. Ho et al. (2003) investigated lower-energy ion and electron data also from the ACE spacecraft. In five out of nine impulsive events the ion release times were delayed compared to electrons, while in four events the release times agreed within the uncertainties. However, no correlation of the two types of events with the ^{3}He/^{4}He ratio was observed. Finally, Tylka et al. (2003) examined two large impulsive SEP events and three ground level events by using electron and ion data from several spacecraft and ground level cosmic ray data from neutron monitor stations. In the impulsive events, the particle release times coincided with hard X-ray emission onsets, but the ground level events showed delayed release with respect to γ-ray emission. The results were interpreted as differences in particle acceleration mechanisms in the two types of events.

When determining release times of solar energetic particles at the Sun from observations near the Earth, two different problems related to the exact timing of the events are encountered. First, one has to define the onset of the event at 1 AU in several energy channels. As a criterion of the onset, one can use the rise of the particle intensity above the pre-event average background by a certain factor expressed in the units of the statistical error of the pre-event counting rate (e.g., Krucker et al. 1999; Tylka et al. 2003). Haggerty & Roelof (2002) have refined this method by introducing a quality factor defined in terms of the difference between the pre-event background and the maximum intensity of the event in the units of the statistical error of the pre-event counting rate. The defined quality factor was shown to indicate the moment of time when the vast majority of the rise of intensities was observed, and thus provide a satisfactory statistical measure of the quality of the onset. An other procedure is to use the cumulative sum method to calculate the normalized time-integrated excess of counting rate above the background level (Torsti et al. 1998). Still another method is to define the onset as increase of the intensity above a fixed fraction of the maximum intensity of the event. The latter is essentially applied in the technique presented by Ho et al. (2001), in which velocity (energy per nucleon) vs. time scatter plots of pulse height data are analysed. The event onset at 1 AU at various energies is determined by fitting a Gaussian distribution to the pulse height data and defining the two-sigma point prior to the maximum as the onset time.

The second step in the analysis is to deduce the release time of the particles at the Sun based on the observed onset time at 1 AU. Two basic methods have been applied. It may be assumed that the path length of all particles along the magnetic field line from the acceleration site to the observation site is fixed, corresponding to the nominal path length along the Archimedean spiral in the appropriate solar wind conditions. Based on this path length and the observed onset time at 1 AU, the release times of particles at the acceleration site near the Sun can be calculated at various energies (e.g., Kahler 1994; Haggerty & Roelof 2002). Justification for this approach is based on the arguments that the first identified particles from a solar event are those which have the cosine of the pitch angle $\mu \sim 1$, and have undergone no or almost no scattering. The second method assumes a linear dependence between the inverse velocity of the particles and the observed onset time at 1 AU (Torsti et al. 1998; Krucker et al. 1999; Mewaldt et al. 2003; Tylka et al. 2003; Ho et al. 2003), which allows the solar release time and the particle path length to be obtained as fitting parameters. This method is also known as the velocity dispersion analysis. Both methods of course suffer from the uncertainties and effects caused by the source location, particle injection profiles, and conditions in interplanetary space during propagation. Recently, Lintunen & Vainio (2004) analyzed SEP event onsets from simulated data with the purpose of evaluating the capabilities of the velocity dispersion analysis. Effects of different coronal and interplanetary scattering conditions of protons were simulated. It was concluded that the best timing results by using the velocity dispersion analysis are obtained for events with interplanetary mean free paths $\gtrsim$0.3 AU and clear intensity increases above the pre-event background.

In this paper, we investigate the proton and helium onsets in SEP events in order to study the solar release times of these species relative to each other and to other SEP-related phenomena. A new method, based on a statistical quality control scheme (Poisson-CUSUM), is presented for defining the event onset time at 1 AU. Velocity dispersion analysis is applied for deducing the release time of the particles at the Sun assuming the same path length for both species.

The paper is organised as follows. The event selection and data sources are briefly described in Sect. 2. Section 3 is devoted for describing the method of onset time determination. The discussion about inferring the solar release times of the particles is presented in Sect. 4. Results and analysis are given in Sect. 5, and finally discussion and conclusions in Sect. 6.

2. Data

In this study, we use the energetic particle data from the SOHO/ERNE (Torsti et al. 1995) High Energy Detector (HED) for the analysis. HED has a high sensitivity (Valtonen et al. 1997), and thus detects also small particle events. The study covers the period between May 8, 1996 and June 20, 2001. The identification of protons and helium nuclei is based on an on-board algorithm, which provides proton and helium counting rates in the energy range ∼12−140 MeV/n with 1-min time resolution. The particle data is accessible through the Erne Datafinder application, which can be found at `http://www.srl.utu.fi/erne_data/`. We determine the apparent release times of the particles at the Sun using six energy channels in the range of ∼14−51 MeV/n. For a SEP event,

we required that a rise above the pre-event background of the helium intensities had to be visible at all the six energy channels. This event selection criterion narrows down the number of selected events. Another requirement was that the corresponding proton event onset had to exhibit a clear velocity dispersion. In some events, the helium counting rates were low, obscuring the velocity dispersion in statistical fluctuations. However, in order to increase the event statistics, we accepted these events in the analysis, i.e., a clear velocity dispersion was not required for the helium channels. In addition, we rejected a number of events due to data gaps or high backgrounds from previous events. We found a total of 25 proton/helium events fulfilling these selection criteria (see Table 2).

3. Method of onset time determination

We apply a statistical quality control scheme in the onset time analysis of the SEP events. In this scheme, we consider a SEP event with a steady pre-event background followed by an increase in the intensity analogous to an industrial process drifting out of control. The task of a statistical quality control is to decide whether or not the process is in control, and if not, the quality test should give the exact moment of time when the failure (SEP event onset) happened. In the SEP event analysis, a one-sided scheme of failure is required, because the intensity is expected to increase only. Another characteristic of the SEP onset analysis is that the "quality control" can be performed offline. Therefore, when the quality control scheme gives an out-of-control signal, the behaviour of the following data points can be inspected and the validity of the out-of-control signal can be verified.

Cumulative sum (CUSUM) quality-control schemes were proposed by Page (1954). CUSUMs for variables are widely used in industry, because they are designed to give an early indication of process changes (Lucas 1985). Traditional cumulative sum methods rely upon assumptions that the quantity being monitored is normally distributed, and that the variable exhibits no serial autocorrelation (Rogerson & Yamada 2004). When the variable being monitored has a Poisson distribution, a Poisson-CUSUM should be used (Lucas 1985). In this work, we will make use of a Poisson-CUSUM to define the event onset time.

A cumulative sum control scheme cumulates the difference between an observed count Y_i and a reference value k. If this cumulation equals or exceeds the decision interval value h, an out-of-control signal is given. For a Poisson-CUSUM used to detect an increase in counts (one-sided scheme), the CUSUM statistic is

$$S_i = \max(0, Y_i - k + S_{i-1}). \quad (1)$$

A standard CUSUM will have a starting value $S_0 = 0$ (Lucas 1985).

For a Poisson-CUSUM, the k value will be chosen to be between the acceptable process mean (μ_a) and the mean level of counts (μ_d), which the CUSUM scheme is to detect quickly. Here μ_a and μ_d are the mean numbers of counts per sampling interval (Lucas 1985).

The reference value for the Poisson-CUSUM should be selected to be close to

$$k = \frac{\mu_d - \mu_a}{\ln(\mu_d) - \ln(\mu_a)}. \quad (2)$$

If μ_a is zero, the CUSUM is designed with $h = 1$ and $k = 0$; any occurrence of a count gives a signal. When $k \geq 1$, the k value will usually be rounded to the nearest integer (Lucas 1985).

In this work, we will estimate μ_a for each event and each energy channel using pre-event background values. Appropriate time intervals for the pre-event backgrounds are chosen with a look-up procedure from the intensity-time profiles. It is also possible to implement an algorithm that estimates μ_a using a sliding average, which is a suitable approach when the pre-event background drifts downwards. There is no standard rule for choosing μ_d value. We will use a two-sigma-shift criterion:

$$\mu_d = \mu_a + 2\sigma_a, \quad (3)$$

where σ_a is the standard deviation of the pre-event background (μ_a).

Because we want to identify the event onset as soon as possible from the particle counting rates, we have chosen a very small decision interval value h:

- if $k < 1$, then $h = 1$;
- if $k \geqslant 1$, then $h = 2$.

The small h value results in a high probability of "false alarm" of event onset. Therefore, we will apply an additional requirement for an event onset: more than one out-of-control signal is required in a row. The following criterion is applied: if an out-of-control signal is detected, then the next 29 Poisson-CUSUM values will be checked as well. If there are 30 out-of-control signals in a row, the first out-of-control signal is defined as the event onset time.

Figures 1 and 2 illustrate the Poisson-CUSUM method in the case of November 4, 1997 event in the energy channel 20.8−28.0 MeV/n. For the pre-event background intervals of proton and helium channels we selected 05:00−06:20 UT and 00:00−05:00 UT, respectively. The average counting rates in these time intervals were taken as parameters μ_a(p) and μ_a(He). The parameters μ_d(p) and μ_d(He) were then calculated from Eq. (3), and the k values from Eq. (2). For protons we obtain k(p) = 8.4 min^{-1} and for helium k(He) ≈ 0.82 min^{-1}, resulting in the decision interval values h(p) and h(He) of 2 and 1, respectively.

The Poisson-CUSUM processes for the proton and helium channels were evaluated from Eq. (1). They are presented with filled diamonds in Figs. 1 and 2, for the proton and helium channels, respectively. Actual counting rates (open triangles), parameters μ_a (dashed, horizontal line) and μ_d (dotted, horizontal line), and decision interval values h (solid, horizontal line) are also presented in the figures. The y-axes of the plots are logarithmic. The first out-of-control value that meets the 30-in-a-row rule is marked with a circle. This moment of time is defined as the event onset.

It is clearly seen in Figs. 1 and 2 how the decision interval value h is related to false alarms and to a delayed observation of the onset. Before the event onsets, there are out-of-control signals occasionally (diamonds that are on or over

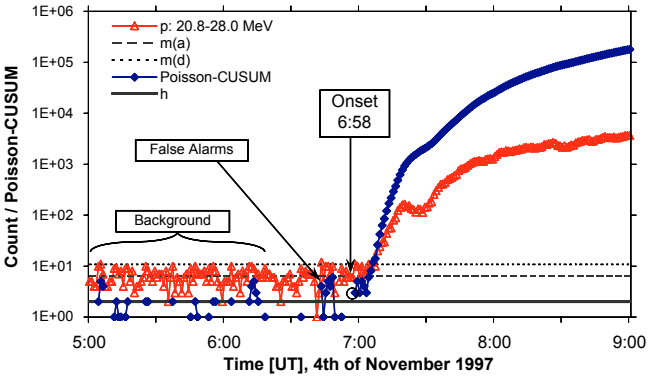

Fig. 1. The proton counting rates (triangles) and Poisson-CUSUM process (diamonds) for the November 4, 1997 event using the energy channel 20.8−28.0 MeV. Time resolution is one minute. The pre-event background level (parameter $\mu_a = m(a)$) is shown with the dashed horizontal line, and the two-sigma upper limit for the background level (parameter $\mu_d = m(d)$) with the dotted horizontal line. The solid horizontal line represents the decision interval value (h) for the Poisson-CUSUM. The circled Poisson-CUSUM value is defined as the event onset.

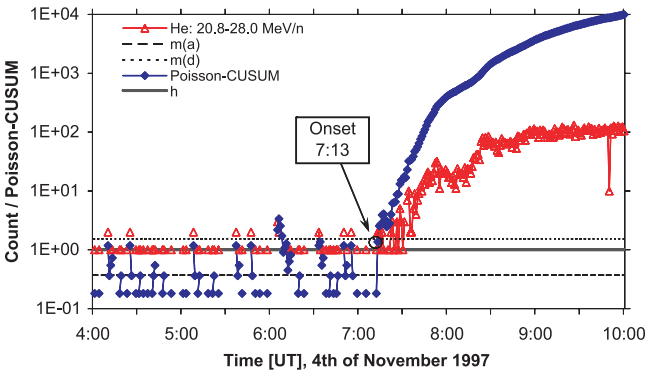

Fig. 2. Same plot as in Fig. 1 but for helium.

the solid horizontal line). All the out-of-control signals that precede the actual event onset are false alarms. If one would choose larger h value (say, $h = 10$ in Fig. 1) there would of course be less false alarms (none in Fig. 1), but the probability of a delayed onset observation would increase. It is note-worthy that the requirement for 30 out-of-control signals in a row is crucial, because it eliminates efficiently false alarms. For using the method demonstrated above, the prerequisite of at least a short duration of "steady" pre-event background is also applicable in order to estimate the k value.

4. Inferred release times

An observed velocity dispersion at 1 AU is regarded as a signature of SEP events. Assuming that particles with different energies are released simultaneously at or close to the Sun, the onset of the event at 1 AU should be observed earlier at higher energies than at lower ones. Assuming further that the energies of the particles remain unchanged through the passage in interplanetary space and that the path length does not depend on energy, it is possible to infer the release time of particles at the Sun and the path length travelled. The velocity dispersion equation at 1 AU is

$$t_{\rm onset}(E) = t_0 + 8.33 \frac{\rm min}{\rm AU} \cdot s \cdot \beta^{-1}(E), \quad (4)$$

where $t_{\rm onset}(E)$ is the observed onset time [min] at energy E, t_0 is the release time [min] from the acceleration site, s is the path length [AU] travelled by the particles, and $\beta^{-1}(E) = c/v(E)$ is the inverse velocity of the particles.

Nominally, the path length should be close to the length of the Archimedean spiral from the Sun to the Earth (~1.2 AU), but many velocity dispersion studies (e.g., Debrunner et al. 1997; Torsti et al. 1998; Krucker & Lin 2000) have shown that there can be large variations in the path lengths obtained from Eq. (4). In one part, Lintunen & Vainio (2004) have related the observed path length variations to changing conditions in interplanetary scattering conditions. On the other hand, Haggerty & Roelof (2003) have shown that instrumental effects can be a cause for too small apparent path lengths. Nevertheless, in this work the release times of protons and helium nuclei are determined by using the velocity dispersion analysis. We regard this as reasonable, because the primary goal of the study is to compare the release times of protons and helium nuclei to each other, and we assume the same path length for both species. In this approach, the accuracy of the apparent path length is not important. The possible consequences of the above mentioned uncertainties are discussed in Sect. 6.

In the velocity dispersion analysis, the proton event onset times ($t_{\rm onset}$) are first determined at six energy channels between 14−51 MeV/n using the Poisson-CUSUM application described in Sect. 3. Based on the determined onset times and the known proton velocities at each energy channel, the velocity dispersion fit according to Eq. (4) is then carried out to obtain the apparent release time ($t_{0,\rm p}$) and path length ($s_{\rm p}$) of protons. Subsequently, the corresponding helium event onset times are determined at the equivalent energy per nucleon channels as for protons. The helium channel onset times are then shifted back in time assuming that helium nuclei in the SEP event have the same path length $s_{\rm p}$ as protons. The average shifted onset time is defined as the apparent release time ($t_{0,\rm He}$) of helium nuclei. The uncertainty of $s_{\rm p}$ is also reflected in the error limits of $t_{0,\rm He}$. Finally, $t_{0,\rm p}$ and $t_{0,\rm He}$ are compared. The delay of helium nuclei compared to protons is defined as

$$\Delta \equiv t_{0,\rm He} - t_{0,\rm p}, \quad (5)$$

where Δ is given in minutes. If Δ is consistent to zero within the error limits, the event is defined as "non-delayed". Otherwise it is defined as "delayed".

5. Results and analysis

5.1. Detailed analysis of two example events

The events of November 4, 1997 and April 4, 2000 are taken as examples to illustrate the analysis of the release times of protons and helium nuclei.

First, the onset times at six energy channels are determined with the Poisson-CUSUM application as demonstrated

Table 1. Observed and shifted onset times at six energy channels (nominal energies in parentheses) for the example events, and the calculated (apparent) release times and delays.

Event	4.11.1997				4.4.2000			
Onset time [UT]	Observed ($t_{\rm onset}$)		Shifted		Observed ($t_{\rm onset}$)		Shifted	
Path length $s_{\rm p}$ [AU]			1.40 ± 0.15				1.19 ± 0.13	
Energy channel [MeV/n]	p	He	p	He	p	He	p	He
13.8–16.9 (15.4)	7:15	7:36	6:10	6:31	16:23	16:23	15:28	15:28
16.9–22.4 (18.9)	7:08	7:21	6:09	6:22	16:13	16:22	15:23	15:32
20.8–28.0 (23.3)	6:58	7:13	6:05	6:20	16:10	16:12	15:25	15:27
25.9–32.2 (29.0)	6:56	7:18	6:08	6:30	16:08	16:19	15:27	15:38
32.2–40.5 (36.3)	6:54	7:08	6:11	6:25	16:03	16:10	15:26	15:33
40.5–50.8 (45.6)	6:47	7:05	6:08	6:26	15:58	16:11	15:25	15:38
Release time $t_{0,\rm p/He}$ [UT]			$6:08 \pm 6$	$6:26 \pm 7$			$15:26 \pm 5$	$15:33 \pm 7$
Delay Δ [min]			18 ± 10				7 ± 9	
			$\Rightarrow$ "Delayed"				$\Rightarrow$ "Non-delayed"	

in Figs. 1 and 2 for the 20.8−28.0 MeV/n channel of protons and helium, respectively, in the November 4, 1997 event. The observed onset times for all applied energy channels in the two events are given in Table 1.

The apparent path length ($s_{\rm p}$) and release time ($t_{0,\rm p}$) of protons are obtained from the least squares fits of Eq. (4), where β^{-1} is calculated for each channel using its nominal energy (see Table 1). The observed helium onset times are then shifted back in time by subtracting from the observed onset times the time-of-flight corresponding to the path length $s_{\rm p}$, giving the apparent release time of the helium nuclei. The results are presented in Table 1.

Finally, the delay Δ is obtained from Eq. (5). As can be seen in Table 1, the November 4, 1997 event is according to our definition "delayed", while the April 4, 2000 event is "non-delayed" (Δ is consistent to zero within the error limits).

The SOHO/ERNE counting rates in these example events are presented in Figs. 3 and 4. To better illustrate the technique, the graphical representation of the two events are different from one another. The counting rates in the April 4, 2000 event are plotted as a function of observed time demonstrating the observed velocity dispersion (Fig. 3). The counting rates at each energy channel for protons and helium are presented in the same panels. From the figure, it is evident that the proton and helium onsets occur simultaneously within the error limits ("non-delayed" event). Figure 4 displays the counting rates in November 4, 1997 event with shifted time axis, corresponding to the estimated release time of particles at the Sun. In this presentation, the onsets take place roughly at the same time for all the proton channels and helium channels, respectively. For clarity of presentation, the proton and helium channels are separated, proton channels being the six uppermost plots. The observed, shifted onset times are indicated by the thick short lines. The derived release times of protons and helium are marked with the dashed vertical lines and their error limits with the thin vertical lines. In this event, the helium nuclei are apparently released later than protons ("delayed" event).

It should be noted, that the curves in Figs. 3 and 4 represent the counting rates of observed particles, not the real intensities. Thus, the figures only serve to demonstrate the two type of events discovered in this work. A detailed discussion of these two and the other events follows later.

5.2. Apparent path lengths, release times, and delays

The velocity dispersion analysis and release time comparisons of protons and helium nuclei were performed for 25 SEP events. The derived apparent path lengths, proton and helium nuclei release times at the Sun, and the calculated delays (defined in Eq. (5)) are given in Table 2. As we are not performing real-time forecasting of the event onset, we have taken advantage of the possibility to visually verify the Poisson-CUSUM method. As a result, in some events we allowed a few in-control signals during the required 30-min e control period for some isolated energy channels, if the velocity dispersion analysis using the other energy channels in the event supported such a decision.

In Table 2, the events with a delay consistent to zero within the error limits are marked with an asterisk. The rest of the events are defined as "delayed". Table 2 also contains rough estimates of the quality of the observation of the helium velocity dispersion, although a clear observed velocity dispersion for helium was not a criterion for the event selection. "Good" velocity dispersion refers to an expected behaviour of the onset times, i.e., the onset at 1 AU occurs earlier at higher energies than at the lower ones. "Scattered" refers to a situation, where the determined onsets have random variations at different energy channels. "Backward" means that the onset occurs earlier at lower energies than at higher ones. This can also be "partial", indicating a change in the slope of the observed velocity dispersion. A "scattered" and "(partly) backward" observed velocity dispersions are probably caused by low statistics in the counting rates, which is a difficult problem for any onset time determination method. It should be

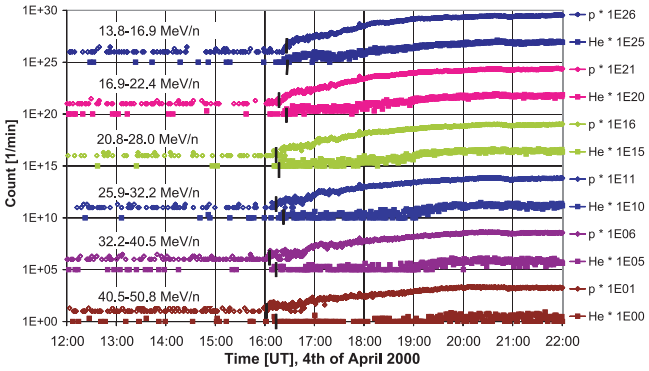

Fig. 3. An example of "non-delayed" event (April 4, 2000). The figure shows in different panels the counting rates at six different energy channels for protons and helium nuclei. The onset times are marked with short, thick vertical lines. To separate the counting rates from each other, different series have been multiplied by suitable constants. The corresponding proton and helium channels are presented in the same panels. The time series are plotted in observed time so that the velocity dispersion is visible.

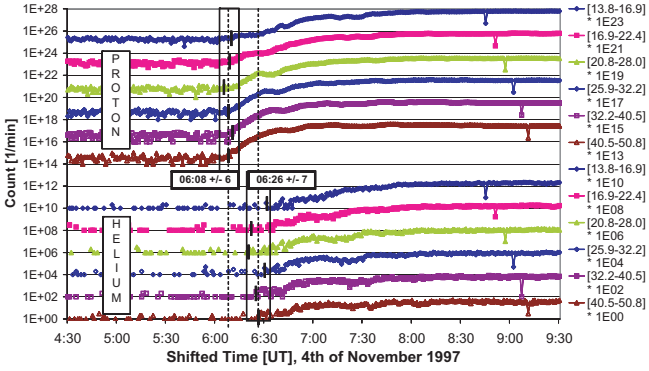

Fig. 4. An example of "delayed" event (November 4, 1997). As in Fig. 3, the counting rates have been multiplied by different constants. Proton and helium channels are presented in different panels. The time series are plotted in shifted time by using the path length $s = 1.40$ AU obtained from the velocity dispersion of protons. The onset times are marked as in Fig. 3. The dashed vertical lines represent the release times of protons and helium nuclei and the solid lines their error limits.

emphasized that the quality estimates are only valid for the studied energy range (14−51 MeV/n).

The distribution of the apparent path lengths (s_p) derived for protons in the 25 SEP events listed in Table 2 is represented in Fig. 5. The average value of all the events is 1.40 ± 0.69 AU, and the median is 1.27 AU. As can be seen in the figure, most of the events (52%) exhibit apparent path length in the range 1.0−1.5 AU. According to Lintunen & Vainio (2004), apparent proton release times for these events should correspond rather well (within a few tens of minutes) to the actual start time of the injection. Large values of the interplanetary mean free path (>0.3 AU) should apply for these events. There are also six events (24%) which have apparent path length <1 AU. These may be due to instrumental effects leading to identification of high energy protons as lower energy ones. The distribution shows also six events (24%) having apparent path length 1.5−3.5 AU. These long path lengths may be caused by stronger interplanetary scattering (Lintunen & Vainio 2004). More detailed discussion on the reasons and the effects to the delays of these non-nominal path lengths is given in Sect. 6.

The distribution of the apparent proton path lengths (Fig. 5) determined for the 25 SEP events in this work do not show a similar behaviour as the results of Krucker & Lin (2000). Analysing Wind electron and proton data in the energy range 30 keV−6 MeV, Krucker & Lin (2000) discovered two classes of solar proton events. In the first class the apparent path length for electrons and protons was the same, $s_{e/p} \approx 1$ AU, while in the second class the path lengths for electrons and protons were different: $s_e \approx 1$ AU and $s_p \approx 2$ AU. In our sample of events such distribution is not visible (Fig. 5).

Figure 6 presents the distribution of observed delays. As in Table 2, the events are divided into two groups. "Delayed" events are further divided into two subgroups: "delayed(y)" ≡ helium events exhibiting a "good" velocity dispersion, and "delayed(n)" ≡ rest of the events. The average delay of all the delayed events is 34 ± 18 min, and the median is 30 min. The variation in the quality of the observed helium velocity dispersion spreads the distribution towards larger delays. The reason for this is obvious. A "backward" velocity dispersion implies that the onsets are observed too late at the highest energy channels, and this causes additional apparent delay when comparing the helium and proton release times to each other. The average delay of the "delayed(y)" events is 27 ± 17 min (median: 18 min), and of the delayed(n) events 42 ± 17 min (median: 35 min). These averages are indicated in Fig. 6 by the arrows.

For confirmation of the results, it is useful to focus only on the more reliable events. There is a total of nine events (1, 4, 7, 10, 12−15, and 18) that possess an apparent path length between 1.0 AU and 1.5 AU, and, on the other hand, show a good velocity dispersion for helium nuclei. Four of these (44%) are "non-delayed", and five (56%) "delayed". The average delay of these "delayed" events is 25 ± 12 min (median: 18 min), which is comparable to the average delay of "delayed(y)" events that do not have any restriction on the used apparent path length.

It should be noted, that only one event (4% of all) in Fig. 6 has a negative delay. Taking the error limits into account, this event is defined as "non-delayed". Altogether, 32% of all the events (8/25) are defined as "non-delayed" and 68% (17/25) as "delayed". Therefore, in the events studied here, helium nuclei are always released at the same time or later than protons, and never before.

5.3. Characteristics of delayed and non-delayed events

Possible reasons for the observed delays in helium release times compared to protons can be studied by comparing the two dissimilar groups of events. The splitting of the events into "non-delayed" and "delayed" events can be contradicted when looking at the delay distribution in Fig. 6. It can be argued that a threshold delay of ~25 min could better divide the events into two different groups. It must be realized, however, that the events with $\Delta > 25$ min are mostly those, which do not exhibit a clear velocity dispersion for helium nuclei. Without the

Table 2. Apparent path lengths, release times, and delays in the 25 events studied.

Event	Date	Path length	Release time [UT ± min]		Delay	Comment on helium
#	dd.mm.yyyy	s_p [AU]	Proton $t_{0,p}$	Helium $t_{0,He}$	Δ [min]	velocity dispersion (at 14–51 MeV/n)
1	04.11.1997	1.40 ± 0.15	6:08 ± 6	6:26 ± 7	18 ± 10	good
2	13.11.1997	1.74 ± 0.16	21:42 ± 6	22:39 ± 22	57 ± 23	(partly) backward
3	20.04.1998	1.05 ± 0.12	10:48 ± 5	11:28 ± 15	40 ± 16	(partly) backward
4	02.05.1998	1.21 ± 0.48	13:36 ± 2	13:51 ± 4	15 ± 5	good
5*	06.05.1998	0.72 ± 0.08	8:14 ± 3	8:16 ± 4	2 ± 5	good
6	09.05.1998	2.37 ± 0.09	3:30 ± 4	4:26 ± 15	56 ± 16	good
7*	27.05.1998	1.36 ± 0.22	13:41 ± 9	13:46 ± 10	5 ± 14	good
8	18.10.1998	1.86 ± 0.21	21:29 ± 8	22:15 ± 40	46 ± 41	(partly) backward
9	24.04.1999	0.48 ± 0.06	14:20 ± 3	14:47 ± 4	27 ± 5	scattered
10	27.05.1999	1.27 ± 0.07	10:48 ± 3	11:05 ± 7	17 ± 8	good
11*	28.12.1999	3.10 ± 0.23	0:37 ± 9	0:44 ± 32	7 ± 34	scattered
12	17.02.2000	1.49 ± 0.25	20:38 ± 10	21:18 ± 19	40 ± 22	good
13	02.03.2000	1.38 ± 0.05	8:38 ± 2	9:13 ± 9	35 ± 10	good
14*	04.04.2000	1.19 ± 0.13	15:26 ± 5	15:33 ± 7	7 ± 9	good
15*	01.05.2000	1.08 ± 0.21	10:19 ± 7	10:20 ± 8	1 ± 11	good
16	10.06.2000	0.78 ± 0.07	17:12 ± 3	17:21 ± 3	9 ± 5	good
17*	15.06.2000	1.22 ± 0.03	19:52 ± 2	19:45 ± 7	–7 ± 8	scattered
18*	17.06.2000	1.12 ± 0.38	4:21 ± 14	4:23 ± 15	2 ± 21	good
19*	28.06.2000	1.44 ± 0.38	19:04 ± 13	19:11 ± 16	7 ± 21	scattered
20	12.09.2000	1.33 ± 0.11	12:31 ± 4	13:44 ± 32	73 ± 33	(partly) backward
21	16.10.2000	0.72 ± 0.10	7:21 ± 4	7:51 ± 10	30 ± 11	scattered
22	08.11.2000	0.49 ± 0.02	23:08 ± 1	23:38 ± 7	30 ± 8	scattered
23	28.01.2001	2.76 ± 0.24	15:49 ± 9	16:28 ± 11	39 ± 15	good
24	29.03.2001	2.68 ± 0.31	9:42 ± 12	10:12 ± 22	30 ± 26	scattered
25	18.04.2001	0.89 ± 0.07	2:42 ± 3	2:54 ± 7	12 ± 8	good

*Defined as "non-delayed".

"delayed(n)" group events, the dip at [20−30) is negligible, when considering statistics of the distribution.

In this work, the "non-delayed" and "delayed" events are chosen to be the comparison groups whose properties are compared mainly with the Student's two sided t-test. The SEP events are characterised by the background intensity, maximum intensity, e-folding rise time, and the time of maximum intensity, all obtained at the energy 13.8−16.9 MeV/n.

Several SEP, CME, and X-ray flare properties, such as apparent path lengths, pre-event background intensities, maximum intensities, e-folding rise time at the beginning of the proton event, the angle between the direction of the interplanetary magnetic field and the sensor field of view direction at the onset, GOES X-ray flare duration and maximum flux, LASCO CME acceleration and central position angle, did not show significant differences ($t < t_{\alpha=0.1}$) between the "non-delayed" and "delayed" events.

The properties that did have differences at the significance level of at least 90% are listed in Table 3. The flare location seems to have a significant role in the "non-delayed" events. All the "non-delayed" events arise from the well-connected area (close to W60). This is illustrated in Fig. 7, which excludes six backside events – all "delayed" cases (see Table 4). There also seems to be a difference in the event rise times to the maximum intensity, and especially in the helium-to-proton ratios at the time of maximum intensities of the "non-delayed" and "delayed" events. The helium-to-proton ratio vs. helium event rise time to the maximum is presented in Fig. 8. In general, the ratio is lower for the "non-delayed" events, and in particular at a

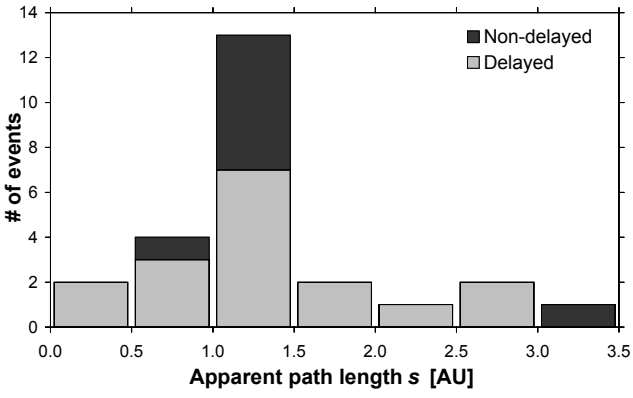

Fig. 5. Proton path length distribution.

Table 3. Differences between the "non-delayed" and "delayed" events.

Property (average)	"Non-delayed"	"Delayed"	Student's $\frac{t}{t_{\alpha=0.05}}$	Significance level
LASCO CME linear speed [km s^{-1}]	1020 ± 260	1320 ± 590	0.838	90%
Flare location longitude (E < 0°, W > 0°)	$66° \pm 12°$	$44° \pm 34°$	0.897	90%
Time from proton onset to maximum [h]	3.8 ± 4.0	7.6 ± 4.9	0.977	90%
Time from helium onset to maximum [h]	3.4 ± 2.4	6.8 ± 4.7	1.15	95%
He/p at event maximum	0.20 ± 0.18	0.013 ± 0.011	1.30	98%
LASCO CME angular width	$160° \pm 110°$	$295° \pm 99°$	1.38	98%
Flare location latitude (S < 0°, N > 0°)	$16° \pm 11°$	$-7° \pm 21°$	1.50	99%
Flare location distance from N20W60 [$R_\odot$]	0.21 ± 0.20	0.76 ± 0.37	1.97	99.9%

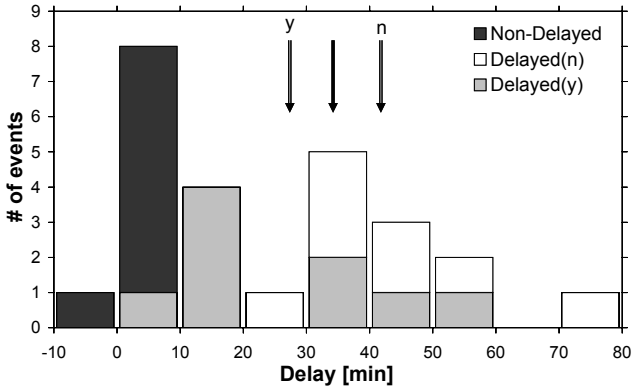

Fig. 6. Delay distribution. Events defined as "delayed" are divided in two groups. "Delayed(y)" correspond to the events exhibiting a "good" velocity dispersion for helium nuclei, and "Delayed(n)" those having a "scattered" (or even "backward") velocity dispersion. The middle arrow marks the average delay (34 ± 18) calculated from all the "delayed" cases, and left/right arrow marks the average delay of the "Delayed(y/n)" cases (27 ± 17 / 42 ± 17).

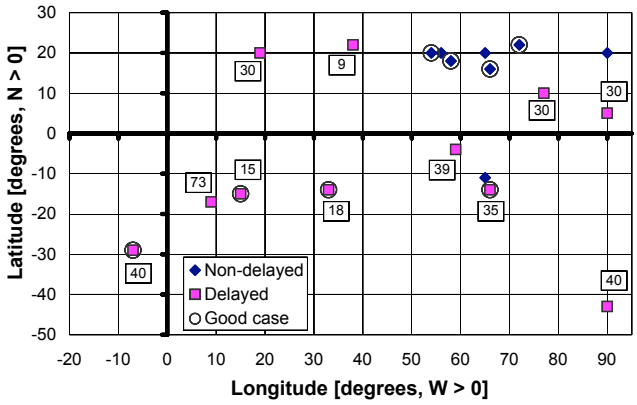

Fig. 7. Locations of flares related to 19 "delayed" and "non-delayed" frontside events. A "Good case" refers to an event that has s = 1.0–1.5 AU and helium nuclei onsets possess a good velocity dispersion. Observed delays in minutes are presented only for the "delayed" events.

fixed rise time. The dashed line in Fig. 8 separates the groups quite nicely, although the event of April 4, 2000 seems to be an exception.

The "non-delayed" and "delayed" events also exhibit differences in CME linear speeds and angular widths, as seen in the scatter plot in Fig. 9. Only one event (a backside event, October 18, 1998) seemed to lack a CME. A simple division in two groups cannot be found in this presentation, however, and the dashed line in the figure merely shows that all the "non-delayed" events are associated with CME linear speeds of less than 1400 km s^{-1}. This of course may be a cause of the limited event sample size. Most of the "delayed" events are associated with a full halo CME, while for the "non-delayed" events this is the case only for the event on April 4, 2000. The difference in the CME angular widths has probably no significance, because the distribution of source locations is a sufficient explanation. CMEs originating closer to the disk center appear as full halos with higher probability than those nearer the disk edge (Wang et al. 2002). As can be seen in Figs. 7 and 9, six full halo CMEs connected to "delayed" helium events originate from longitudes ~E10...W40.

Comparison of SEP timing with electromagnetic observations related to the studied events is presented in Table 4. The Table lists some relevant flare and CME data, and radio type II and III-l timing data. In the case of solar backside events (e.g., events 8–10), the given locations of the active regions and the associations of the electromagnetic emissions with the particle events are less reliable than for the frontside events. The backside event associations with the CME, X-ray flare and the radio type III-l observations were obtained from Cane et al. (2002). The radio type II associations were chosen when they were temporally close to the other observations. Eight minutes have been added to the inferred proton release times to make them comparable with the electromagnetic observations. The symbols preceding the release times indicate the presumable "direction" of the actual injection time. The symbols represent the velocity dispersion fitted apparent path length, only. "No symbol" represents events with 1.0 AU $\leq s \leq$ 1.5 AU, and the timing should be quite reliable. The symbols ">" and "$\gg$" indicate $s >$ 1.5 AU and $s \gg$ 1.5 AU, respectively, in which case the presumable actual injection occurred later than given. The symbols "<" and "$\ll$" refer to cases with $s <$ 1.0 AU and $s \ll$ 1.0 AU, and the presumable actual injection occurred earlier than given. Generally, the proton release times agree quite well with the timing of electromagnetic observations. It is

Table 4. X-ray flares, CMEs, Type II and III-*l* radio bursts related to the studied events.

#	Date dd.mm.yy	Proton Release Time[a] + 8 min [UT]	GOES X-ray[b] Class	GOES X-ray[b] start/peak/end [UT]	LASCO CME[e] Flare Location	LASCO CME[e] Lin. speed [km s^{-1}]	LASCO CME[e] 2nd Ord. Start (First Obs.) [UT]	Radio bursts Type II High freq.[f]	Radio bursts Type II WAVES[g]	Type III-*l*[c] at 14 MHz
1	04.11.97	6:16 ± 6	X2.1	05:52/05:58/06:02	S14W33	785	05:45 (06:10)	06:08–06:17 culg	06:00–04:30+	05:55–06:15
2	13.11.97	>21:50 ± 6	?	?	N??W110[c]	546	20:37 (22:26)	–	–	21:15–21:20
3	20.04.98	10:56 ± 5	M1.4	09:38/10:21/11:18	S43W90[d]	1863	09:52 (10:07)	09:56–10:02 svto	10:25–06:00++	~10:00
4	02.05.98	13:44 ± 2	X1.1	13:31/13:42/13:51	S15W15[b]	938	13:37 (14:06)	–	14:25–14:50	13:35–14:00
5*	06.05.98	<8:22 ± 3	X2.7	07:58/08:09/08:20	S11W65[b]	1099	07:48 (08:29)	08:06–08:19 izmi	08:25–08:35	08:00–08:30
6	09.05.98	>3:38 ± 4	M7.7	03:04/03:40/03:55	S??W100[c]	2331	03:29 (03:36)	03:31–03:41 culg	03:35–10:00	03:25–03:50
7*	27.05.98	13:49 ± 9	C7.5	13:30/13:35/14:50	N18W58[b]	878	13:09 (13:46)	–	13:30–14:20	13:15–13:30
8	18.10.98	>21:37 ± 8	?	?	N??W130[c]	?	?	21:12–21:17 culg	23:00–23:15	21:05–21:10
9	24.04.99	≪14:28 ± 3	?	?	S??W150[c]	1495	12:57 (13:31)	–	13:50–24:00	13:00–13:40
10	27.05.99	10:56 ± 3	?	?	S??W120[c]	1691	10:43 (11:06)	10:46–10:57 sgmr	10:55–10:00+	10:45–11:10
11*	28.12.99	≫0:45 ± 9	M4.5	00:39/00:48/00:52	N20W56[b]	672	00:40 (00:54)	00:46–00:55 culg	–	00:40–00:50**
12	17.02.00	20:46 ± 10	M1.3	20:17/20:35/21:07	S29E07[b]	600	19:45 (20:06)	20:38–20:49 culg	20:42–22:12+	20:25–20:40
13	02.03.00	8:46 ± 2	M1.1	08:38/08:41/08:47	S14W66[b]	776	08:06 (08:54)	08:27–08:46 svto	–	08:25–08:35
			(X1.1)	(08:20/08:28/08:31)	(S14W52[c])					
14*	04.04.00	15:34 ± 5	C9.7	15:12/15:41/16:05	N16W66[b]	1188	14:42 (16:33)	15:30–15:32 pots	15:45–16:00	15:15–15:35
15*	01.05.00	10:27 ± 7	M1.1	10:16/10:27/10:34	N20W54[c]	1360	10:22 (10:54)	–	–	10:20–10:25**
16	10.06.00	<17:20 ± 3	M5.2	16:40/17:02/17:19	N22W38[b]	1108	16:51 (17:08)	16:55–17:18 sgmr	17:15–18:45	17:00–17:15
17*	15.06.00	20:00 ± 2	M1.8	19:38/19:57/20:19	N20W65[b]	1081	19:32 (20:06)	19:43–19:46 holl	19:52–19:56	19:45–19:50**
18*	17.06.00	4:29 ± 14	M3.5	02:25/02:37/02:44	N22W72[b]	659	04:03 (04:40)	–	03:00–04:15	~02:30
19*	28.06.00	19:12 ± 13	C3.7	18:48/19:10/19:39	N20W90[e]	1198	18:47 (19:32)	19:03–19:11 holl	–	18:45–19:05
20	12.09.00	12:39 ± 4	M1.0	11:31/12:13/13:13	S17W09[b]	1550	11:39 (11:54)	12:07–12:13 svto	12:00–12:20+	11:45–11:50
21	16.10.00	<7:29 ± 4	M2.5	06:40/07:28/09:11	N05W90[d]	1336	06:46 (07:27)	07:08–07:19 svto	07:10–07:00	~06:50
22	08.11.00	≪23:16 ± 1	M7.4	22:42/23:28/00:05	N10W77[d]	1738	22:46 (23:06)	–	23:20–12:00+	22:55–23:35
23	28.01.01	≫15:57 ± 9	M1.5	15:40/16:00/16:24	S04W59[b]	916	15:42 (15:54)	–	15:45–17:00	15:40–16:05
24	29.03.01	≫9:50 ± 12	X1.7	09:57/10:15/10:32	N20W19[b]	942	09:50 (10:26)	10:03–10:07 izmi	10:12–06:00+	10:00–10:15
25	18.04.01	<2:50 ± 3	C2.2	02:11/02:14/02:16	S??W120[c]	2465	02:12 (02:30)	02:17–02:46 hira	02:55–14:00	02:20–02:40

Notes to table

*defined as "non-delayed".

[a]Eight minutes have been added to make release times comparable with other observations. The symbols preceding the release times indicate the presumable "direction" of the actual injection time. Symbols represent the velocity dispersion fitted apparent path length, only. "No symbol" represents events with 1.0 AU ≤ s ≤ 1.5 AU, and the timing should be quite reliable. The symbols ">" and "≫" indicate s > 1.5 AU and $s \gg 1.5$ AU, respectively, in which case the presumable actual injection occurred later than given. The symbols "<" and "≪" refer to cases with s < 1.0 AU and $s \ll 1.0$ AU, and the presumable actual injection occurred earlier than given.

[b]National Geophysical Data Center (`ftp://ftp.ngdc.noaa.gov/STP/SOLAR_DATA/SOLAR_FLARES/XRAY_FLARES/`).

[c]Cane et al. (2002); Times followed by ** indicate bursts that are likely type III bursts. The remainder are type III-*l*. Single times preceded by a "~" are ones in which there is no emission at 14 MHz and the time is the start time at 1 MHz.

[d]LWS CDAW 2002 Data List (`http://cdaw.gsfc.nasa.gov/LWS/data/event_list.html`).

[e]SOHO LASCO CME CATALOG (`http://cdaw.gsfc.nasa.gov/CME_list`).

[f]National Geophysical Data Center (`ftp://ftp.ngdc.noaa.gov/STP/SOLAR_DATA/SOLAR_RADIO/SPECTRAL/`); Observatories: culgCulgoora (18–1800 MHz), svtoSan Vito (25–75 MHz), izmiIZMIRAN (25–270 MHz), sgmrSagamore Hill (30–80 MHz), potsPotsdam (40–100 MHz), hollHolloman Air Force Base (25–180 MHz), and hiraHiRAS (25−2500 MHz). Bursts are not necessarily observed at the whole frequency range of the given instrument.

[g]Wind/WAVES homepage (`http://lep694.gsfc.nasa.gov/waves/waves.html`); One "+"-sign following the end time means that given end time is on the next day (two signs: on the day after next).

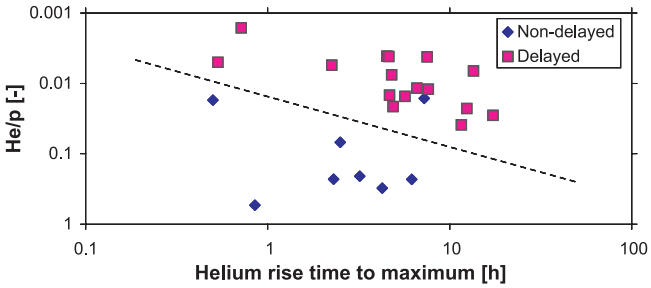

Fig. 8. Helium-to-proton ratio at the intensity maximum vs. helium event rise time to the maximum.

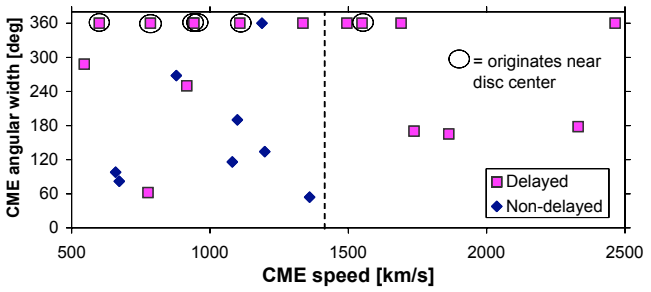

Fig. 9. CME angular width vs. CME linear speed.

noteworthy that the release times in the proton events exhibiting an apparent path length s_p between 1.0 AU and 1.5 AU agree better with the electromagnetic observations than the release times in the rest of the proton events. This conclusion is based on the following score calculation: if the tabulated proton release time is inside the given start time and end time of other observations, one point is scored for that event. The first observation time of a CME is regarded as the "end time" of that observation. Observations with missing data and type III-*l* having only a start time (at 1 MHz) are excluded from the statistics. For example, the event 18 scored one out of three available observations (CME timing gave one point), and the event 20 scored two out of five (GOES and WAVES timings). Total score for the events having $s_p = 1.0 \ldots 1.5$ AU is $\frac{31}{55} = 57\%$, and the rest of the events scored $\frac{20}{49} = 41\%$. This is consistent with the conclusion of Lintunen & Vainio (2004), if we assume that the timings of the electromagnetic observations in Table 4 describe the actual timing of the particle injection. The apparent release times obtained by Lintunen & Vainio (2004) from their simulated data corresponded rather well to the actual start time of the injection times, and such events could be identified from the observational data having values of $s_p \lesssim 1.5$ AU.

When using only the nine events (1, 4, 7, 10, 12–15, and 18), that have apparent path length between 1.0 AU and 1.5 AU, and show a good velocity dispersion for helium nuclei, the analysis yields lower significance levels, most likely due to considerably lower statistics. However, as seen in Fig. 7, the spatial separation of the "delayed" and "non-delayed" event source locations is still apparent.

In addition to the analyses presented above, the apparent proton release heights were determined for 13 events with the most reliable release times (taken as those with deduced $s_p = 1.0 \ldots 1.5$ AU). The release height (in $R_\odot$ above the photosphere) of particles was assumed to be the height of the associated CME at the deduced particle release time. The CME heights were estimated visually from the 2nd order fits of the height vs. time plots of the SOHO/LASCO observations (see SOHO LASCO CME CATALOG: `http://cdaw.gsfc.nasa.gov/CME_LIST/`). No geometrical corrections were performed. No significant difference was found between the proton release heights of the "delayed" and "non-delayed" events. The sample sizes, however, are quite limited. The proton release heights for all the 13 events ranged between $\sim 1\, R_\odot$ and $\sim 9\, R_\odot$.

5.4. Interpretation of observed delays as an instrumental background effect

The differences in the helium-to-proton ratios and the helium event rise times from onset to the maximum intensity of the "non-delayed" and "delayed" events may lead one to suspect that the observed delay is an instrumental effect related to the pre-event background or to the sensitivity of the instrument. Yet, it seems peculiar that the event rise time from the onset to the maximum showed a significant difference (protons 90%, and helium nuclei 95% confidence level), but the e-folding rise time at the beginning of the proton event did not. Clearly the e-folding rise time should better describe the background crossing (onset) than the overall rise time from the onset to the maximum.

If the helium-to-proton ratio for the SEP event stays constant at the beginning, that is, the e-folding rise time is the same for both species, the expected delay can be written as

$$D(a) = \frac{\tau}{\log e}\left(\log\left(\frac{I_{\rm bg}^{\rm He} + a\cdot\sigma_{\rm bg}^{\rm He}}{I_{\rm bg}^{\rm p} + a\cdot\sigma_{\rm bg}^{\rm p}}\right) - \log\left(\frac{I_{\rm sep}^{\rm He} - I_{\rm bg}^{\rm He}}{I_{\rm sep}^{\rm p} - I_{\rm bg}^{\rm p}}\right)\right), \quad (6)$$

where τ is the e-folding rise time, $I_{\rm bg}^{\rm He[p]}$ is the background intensity of the helium [proton] flux, $\sigma_{\rm bg}^{\rm He[p]}$ is the standard deviation of the background, and $I_{\rm sep}^{\rm He[p]}$ is the observed helium [proton] intensity of the SEP event determined at some appropriate time after the onset. We can argue that an event onset may be observable after $I_{\rm sep}^{\rm He[p]}$ has reached some level $I_{\rm bg}^{\rm He[p]} + a\cdot\sigma_{\rm bg}^{\rm He[p]}$, based on statistical variation of the background. Therefore the moments of onsets for helium nuclei and protons are controlled by a factor a, which is selected to be the same for both species, for simplicity.

If we choose $a = 0$ and divide the Eq. (6) by τ, we get a dimensionless quantity D/τ, which depends only on the $BG\left(\frac{\rm He}{\rm p}\right)$-to-$SEP\left(\frac{\rm He}{\rm p}\right)$ ratio, where $BG\left(\frac{\rm He}{\rm p}\right)$ is the helium-to-proton ratio of the pre-event background ($I_{\rm bg}^{\rm He}/I_{\rm bg}^{\rm p}$), and $SEP\left(\frac{\rm He}{\rm p}\right)$ is the same for the SEP event (($I_{\rm sep}^{\rm He} - I_{\rm bg}^{\rm He}$)/($I_{\rm sep}^{\rm p} - I_{\rm bg}^{\rm p}$)). It is reasonable to compare this quantity to the observations. It should be realized, however, that the observed delay is based on the velocity dispersion analysis by using several energy channels, while the characterizing quantities such as τ, $BG\left(\frac{\rm He}{\rm p}\right)$, and $SEP\left(\frac{\rm He}{\rm p}\right)$ are only determined by using

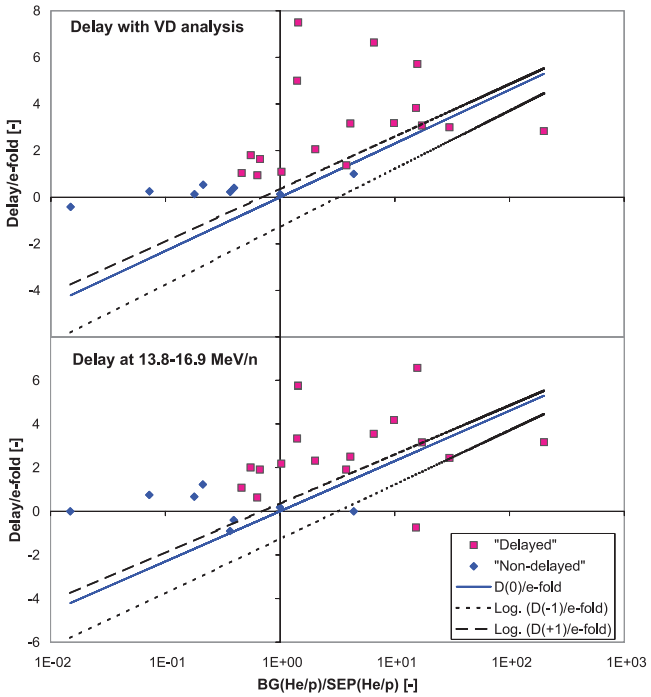

Fig. 10. Comparison between the predicted (Eq. (6)) and the observed delay to e-folding rise time ratios. Filled symbols represent the observed values. Solid inclined line represents the predicted ratio when $a = 0$ in equation 6. Dashed [dotted] line is a logarithmic fit to the predicted values when $a = 1$ [-1]. The upper panel shows the case, when the delays were determined through the velocity dispersion analysis. For comparison, the lower panel shows the delays obtained directly by using the energy channel 13.8–16.9 MeV/n.

one energy channel (13.8–16.9 MeV/n). Figure 10 shows the comparison between the predicted and observed delay-to-e-folding rise time ratios (see the figure caption for details). Only few data points in Fig. 10 could be explained by this simple equation. It also seems to give equally poor results for the "delayed" and the "non-delayed" events. This can be confirmed by the χ^2-test, which gives $\chi^2 = 176$, when $D(0)/\tau$ is used, and 112 for $D(2)/\tau$. The tabulated χ^2 value is $\chi^2_{df=23,\alpha=0.001} = 49.73$. We conclude that this simple equation fails to explain the observations, although a positive a-factor improves the result a little bit. The conclusion remains the same, if the delays would only be determined at the 13.8–16.9 MeV/n energy channel, as shown in the lower panel of Fig. 10.

6. Discussion and conclusions

We utilized the velocity dispersion analysis to determine the apparent solar release times of protons and helium nuclei in SEP events observed with the High Energy Detector of the SOHO/ERNE. The study period was from May 8, 1996 till June 20, 2001. We introduced a statistical quality control scheme (Poisson-CUSUM) for deriving the event onset times at 1 AU from the particle counting rates. The Poisson-CUSUM method proved to be useful in a wide range of signal-to-noise ratios and rise rates of the SEP events. In this study, we used an "off-line" application of the Poisson-CUSUM method, but the method can easily be implemented in a "real-time" onset determination application, being the original idea of a statistical quality control scheme.

In Sect. 5.2 it was noted, that for some events the apparent path lengths, deduced from the 14–51 MeV proton data, turned out to be non-nominal when comparing to the length of the Archimedean spiral (see Table 2 and Fig. 5). The path lengths <1 AU could be due to a similar instrumental effect that was reported by Haggerty & Roelof (2003), who studied the response of the ACE/EPAM instrument to near-relativistic solar electron events. They found that in the case of a hard spectral slope, more high-energy electrons are registered in lower energy channels. Relevant for the onset time study is the rate of the intensity rise and the spectral slope of the pre-event background. If, at the time of the onset, high-energy proton intensity rises very fast, then it could be possible that the "crosswalked" protons can trigger an observable onset at a lower energy channel, which normally has significantly higher background level than the "crosswalking" high energy protons have. To check whether there is such a behavior in the studied events, we determined an e-folding rise time at the beginning of the proton event for the energy channel 13.8–16.9 MeV. It turned out that the apparent path lengths and e-folding rise times correlate with a correlation coefficient of 0.62. We further divided the events into four comparison groups where the apparent path lengths are: (a) $s < 1.0$ AU; (b) 1.0 AU $\leq s \leq 1.5$ AU; (c) $s > 1.5$ AU, and (d) $s \geq 1.0$ AU. The average e-folding rise times in minutes are 6.6 ± 2.5, 14 ± 11, 28 ± 16, and 18 ± 14, respectively. Student's one-sided t-tests showed that with a confidence level of 97.5% the average e-folding rise time for group (a) is smaller than for groups (b) and (c), and with 99.9% confidence level smaller than for group (d). The average for group (b) is also smaller than for group (c), with a confidence level of 95%. Thus, and because the apparent path length distribution in Fig. 5 shows a peak in the nominal range of Archimedean spiral length, we argue that only the events in group (a) are subject to a "crosswalk" of the high energy particles, when considering the onset time analysis. The deduced delays for group (a) events are still comparable to other events, because at least for events 5 and 16 also helium onsets exhibit a clear velocity dispersion that yields $s_{\mathrm{He}} < 1$ AU.

As the above analysis would suggest that a slow rise of the event increases the apparent length of the event, it is tempting to deduce that the slow rise also delays the detection of the onset, and thus affects the measured delays. However, our statistical analysis on the event features and the delay do not support such conclusion, as neither the e-folding time nor the background or maximum intensities of the particle species were found to correlate with the delay. Also the negative result on the instrumental background effect, presented in Sect. 5.4 in its part supports the conclusion that the instrumental effects have negligible influence on the delay measurements.

The longer path lengths (>1.5 AU) may be related to interplanetary scattering of the particles (Lintunen & Vainio 2004). The quasi-linear theory of energetic particle transport suggests that the energetic particle mean free path of the particle, parallel to the magnetic field, scales as the cubic root of rigidity (pc/(Ze)), for Kolmogorov turbulence spectrum. Thus, helium particles traveling with the same velocity as protons would

scatter less efficiently and have shorter effective path length than protons, implying that the delay would decrease with increasing apparent path length. As five of these six long-path-length events, however, are defined as "delayed", we find that this effect does not significantly affect our analysis.

In this study, we found that in eight cases out of 25 (32%) protons and helium nuclei were released simultaneously from the acceleration site, and in 17 cases (68%) the injection of the helium nuclei was apparently delayed when compared to the proton release time. The related flare source location seems to have a significant role in the "non-delayed" events. All the "non-delayed" events arose from a magnetically well-connected region (close to W60) of the Sun, while the "delayed" events were more widely spread on the solar surface. This observation resembles the finding of Krucker et al. (1999), who observed events with delayed and non-delayed electron injection in relation to the onsets of radio type III bursts. As in the present work, although with a different definition of the delay, the non-delayed events of Krucker et al. (1999) were also concentrated in the well-connected regions. The average delay of the "delayed" helium events that exhibited a "good" velocity dispersion was 27 ± 17 min in this study, which is comparable with the delays observed by Krucker et al. (1999) (delays up to 30 min). On the other hand, the proportions of the "non-delayed" and "delayed" events in this work are similar to the result of Krucker & Lin (2000). In eight cases out of 26 SEP events (31%), protons and electrons were injected nearly simultaneously, and in 18 cases (69%) protons were injected ∼0.5−2 h later than electrons (Krucker & Lin 2000). We did not find any difference in the apparent path lengths of protons (s_p) associated with "delayed" or "non-delayed" helium events. Krucker & Lin (2000), on the other hand, reported that proton events delayed with respect to the associated electron events could be distinguished from the non-delayed ones on the basis of the proton path lengths. This indicates that the processes responsible for the delays of helium injection compared to proton injection are different from those causing the delay of proton events with respect to electron events. The different energy ranges of protons used in the two studies (∼14−51 MeV vs. 0.030−6 MeV) may also play a role.

Mewaldt et al. (2003) compared the solar release times of electrons and heavy ions ($Z \geq 6$) for 11 events. They give dates for five of the events, which all have $^3\mathrm{He}/^4\mathrm{He} > 0.02$ and have similar ion and electron release times. Two of those are included in this study (May 6, 1998, and May 1, 2000) and are defined as "non-delayed" events. As an addition to our main analysis, we performed velocity dispersion analysis for the three other events studied by Mewaldt et al. (2003). The event of April 14, 2001 was not included in our study because it showed only minor intensity enhancement on the studied energy range, and the events of February 20, 2002, and August 20, 2002 occurred outside of our study period. The source flare locations were S18W71, N12W72, and S10W38, respectively, so these events originate near the well-connected area. It turned out that the events are "non-delayed" also in regard to proton and helium nuclei release times. Thus, at least in these five cases "non-delayed" events as defined in this work are also "non-delayed" when comparing electron and heavy ion injections.

It is reasonable to consider whether the "delayed" and "non-delayed" events simply correspond to the traditional gradual-impulsive SEP event picture. Current views on impulsive and gradual SEP events are summarized in Kallenrode (2003). In favor of the traditional picture are the following observations: flare longitude distributions ("non-delayed" from the well-connected area), *on average* the helium-to-proton ratio is higher in the "non-delayed" events, and at least in five "non-delayed" events the ^{3}He-to-^{4}He ratio is enhanced (>0.02). The durations of the particle events were difficult to determine, because in several cases there was overlapping of successive events. If the event rise time from the onset to the maximum intensity can be regarded as a measure of the overall duration of the particle event, then it can be said that *on average* the "non-delayed" events have a shorter duration than the "delayed" events. This, again, is a characteristic of the gradual-impulsive picture. On the other hand, it is a well-known fact that the longitude of the flare affects the intensity profile, so that well-connected events rise faster to the maximum intensity (Cane et al. 1988). Against the traditional gradual-impulsive picture are the following observations: there was no difference in the X-ray flare durations in "delayed" and "non-delayed" events, a CME is related to every "non-delayed" event and in two cases (May 27, 1998, and April 4, 2000) even an IP shock is observed (SOHO/CELIAS: May 29, 1998, 14:58 UT, and April 6, 2000, 16:01 UT). Kahler et al. (2001) pointed out that narrow CMEs (10°−40°) can be associated with impulsive SEP events (e.g., May 1, 2000). The average angular width of the CMEs associated with the "non-delayed" events is 160° ± 110°. In one case (April 4, 2000) even a full halo CME was observed. One of the additionally analysed events (February 20, 2002) was also a full halo event. It seems plausible that some of the events in this paper are mixed events which have contributions to high-energy particles from both a flare and a CME (Kallenrode et al. 1992; Kocharov & Torsti 2002).

What causes the observed delay in the apparent solar release times of protons and helium nuclei? There seems to be three options: a) the delay is directly associated to the proportion of the helium-to-proton ratios of the pre-event background and the SEP event and can be regarded as an instrumental effect; b) the delay is related to the magnetic connection between the acceleration site and the observer; or c) something quite different like some propagational effect in interplanetary space, or some combination of different factors.

In Sect. 5.4 we assumed that the helium-to-proton ratio for the SEP event stays constant at the beginning, and failed to explain the observed Δ/τ, where Δ is the observed delay and τ is the e-folding rise time. On the other hand, there seems to be some correlation between Δ/τ and the logarithm of $BG\left(\frac{\mathrm{He}}{\mathrm{p}}\right)$-to-$SEP\left(\frac{\mathrm{He}}{\mathrm{p}}\right)$ ratio. The correlation coefficient based on the data presented in Fig. 10 is 0.574, when the delay is determined with the velocity dispersion analysis, and 0.488, when only one energy channel is used (13.8−16.9 MeV/n). This is a significant correlation, even though one could expect better correlation for the latter than for the former case. This may imply that the possible instrumental effect would be more complex than reasonably assumed in Sect. 5.4, or that a constant helium-to-proton

ratio is not the best assumption. In fact, on one hand the rigidity dependent particle transport predicts a decreasing helium-to-proton ratio for the beginning, and on the other hand proton-amplified waves can lead to an increasing ratio (e.g., Reames et al. 2000). This, together with the possible differences in the proton and helium injection profiles, gives reason to suspect the validity of the assumed constant helium-to-proton ratio.

The observations of Kallenrode (1993) may give a physical viewpoint to the observed delays. Two spacecraft separated in space gave Kallenrode (1993) an advantage to observe the onset of the *same* event at different angular distances. Figure 10 in Kallenrode (1993) gives basically the explanation. At larger angular distances between the observer's magnetic footpoint and the flare location the onsets of electrons and protons in relation to the microwave maximum are more delayed, and the proton onsets are relatively more delayed than the electron onsets. Thus, Kallenrode (1993) concluded that the azimuthal propagation of ~20-MeV protons is systematically slower than ~0.5-MeV electrons, and that the electron-to-proton ratio tends to increase with angular distance. These results correspond to the finding of Krucker et al. (1999). The origins of their non-delayed electron events (compared to onsets of a radio type III emission) were concentrated to the well-connected area, while the delayed events were more spread. On the other hand, Krucker & Lin (2000) found no correlation between the source flare locations and their delayed–non-delayed proton events (compared to electron onsets).

The interpretation of the delay as an azimuthal transport phenomenon, however, is not straightforward. As discussed above, the parallel mean free path for helium is larger than for proton. If we assume that the perpendicular energetic particle transport scales like the parallel transport (e.g., Shalchi et al. 2004), the azimuthal transport should in fact be faster for helium. However, the helium nuclei require more time for the acceleration to the same velocities as protons (e.g., Forman & Webb 1985), which may play an important role for events where the most effective acceleration region is not well connected to the observing spacecraft. The difference of the transport parameters and acceleration times between the species, however, is not large, and may be masked by other phenomena. Thus, further work is needed before a firm interpretation for the delay between helium and proton onsets can be established.

Acknowledgements. This project was supported by the Academy of Finland in the framework of the Antares programme. We acknowledge the use of the CME catalog generated and maintained by the Center for Solar Physics and Space Weather, The Catholic University of America in cooperation with the Naval Research Laboratory and NASA. SOHO is an international co-operation project between ESA and NASA. We thank the referee for valuable comments.

References

Cane, H. V., Reames, D. V., & von Rosenvinge, T. T. 1988, J. Geophys. Res., 93, 9555
Cane, H. V., Erickson, W. C., & Prestage, N. P. 2002, J. Geophys. Res., 107, 14
Dalla, S., Balogh, A., Krucker, S., et al. 2003, Ann. Geophys., 21, 1367
Debrunner, H., Lockwood, J. A., Barat, C., et al. 1997, ApJ, 479, 997
Forman, M. A., & Webb, G. M. 1985, Washington DC American Geophysical Union Geophysical Monograph Series, 35, 91
Haggerty, D. K., & Roelof, E. C. 2002, ApJ, 579, 841
Haggerty, D. K., & Roelof, E. C. 2003, Adv. Space Res., 32, 423
Hilchenbach, M., Sierks, H., Klecker, B., Bamert, K., & Kallenbach, R. 2003, in AIP Conf. Proc., 679; Solar Wind Ten, 106
Ho, G. C., Mason, G. M., Gold, R. E., Dwyer, J. R., & Mazur, J. E. 2001, in Joint SOHO/ACE workshop, Solar and Galactic Composition, AIP Conf. Proc., 598, 353
Ho, G. C., Roelof, E. C., Mason, G. M., Lario, D., & Mazur, J. E. 2003, Adv. Space Res., 32, 2679
Kahler, S. 1994, ApJ, 428, 837
Kahler, S. W., Reames, D. V., & Sheeley, N. R. 2001, ApJ, 562, 558
Kallenrode, M. 1993, J. Geophys. Res., 98, 5573
Kallenrode, M.-B. 2003, J. Phys. G, 29, 965
Kallenrode, M.-B., & Wibberenz, G. 1990, Proc. 21st Int. Cosmic Ray Conf., 5, 229
Kallenrode, M.-B., Cliver, E. W., & Wibberenz, G. 1992, ApJ, 391, 370
Kocharov, L., & Torsti, J. 2002, Sol. Phys., 207, 149
Krucker, S., Larson, D. E., Lin, R. P., & Thompson, B. J. 1999, ApJ, 519, 864
Krucker, S., & Lin, R. P. 2000, ApJ, 542, L61
Laitinen, T., Klein, K.-L., Kocharov, L., et al. 2000, A&A, 360, 729
Lintunen, J., & Vainio, R. 2004, A&A, 420, 343
Lucas, J. 1985, Technometrics, 27, 129
Mewaldt, R., Cohen, C., Haggerty, D., et al. 2003, Proc. 28th Int. Cosmic Ray Conf., 6, 3313
Page, E. 1954, Biometrika, 41, 100
Posner, A., & Kunow, H. 2003, Proc. 28th Int. Cosmic Ray Conf., 6, 3309
Reames, D. V., Ng, C. K., & Tylka, A. J. 2000, ApJ, 531, L83
Rogerson, P., & Yamada, I. 2004, Morbidity and Mortality Weekly Report Suppl., 53, 79
Shalchi, A., Bieber, J. W., & Matthaeus, W. H. 2004, ApJ, 604, 675
Torsti, J., Anttila, A., Kocharov, L., et al. 1998, Geophys. Res. Lett., 25, 2525
Torsti, J., Valtonen, E., Lumme, M., et al. 1995, Sol. Phys., 162, 505
Tylka, A., Cohen, C., Dietrich, W., et al. 2003, Proc. 28th Int. Cosmic Ray Conf., 6, 3305
Valtonen, E., Peltonen, J., Peltonen, P., et al. 1997, Nucl. Instr. Meth. Phys. Res. A, 391, 249
Wang, Y. M., Ye, P. Z., Wang, S., Zhou, G. P., & Wang, J. X. 2002, J. Geophys. Res., 107, 2